CONTROL OF THE OBLIQUE SHOCKWAVE/BOUNDARY LAYER INTERACTION IN A SUPERSONIC INLET

JAMES BELLINGER

THE OHIO STATE UNIVERSITY

MAY 2008

ABSTRACT

In a supersonic engine inlet, the adverse pressure gradient caused by an oblique shockwave generated by an inlet cone interacts with low momentum boundary layer air at the inlet wall to create a region of recirculating flow called a separation bubble. This separated region reduces the effective area of the engine inlet, requiring a larger inlet to get the desired mass flow rate. As a result the engine must be larger and heavier.

Over the past year, investigations have been done into the viability of controlling this oblique shockwave/boundary layer interaction with plasma actuators, using a supersonic wind tunnel simulating an engine inlet. Plasma actuators were considered for this application due to their ability to generate streamwise vortices in the flow. Vortices move low momentum boundary layer air out into the free stream and high momentum free stream air down into the boundary layer, thus increasing the momentum in the interaction region and reducing or eliminating separation.

A test section containing a 10° shock generator and adjustable floor was designed and installed into an existing supersonic wind tunnel. Plasma actuators were tested at various frequencies and distances to the oblique shock impingement point, and their effect was visualized using schlieren photography.

ACKNOWLEDGEMENTS

I would like to thank Professor Mo Samimy, Edgar Caraballo, Jin-Hwa Kim and everyone else at the Gas Dynamics and Turbulence Laboratory, without whom this research would not have been possible. I would also like to thank the Air Force Research Laboratory for their support of this research.

CONTENTS

TABLE OF FIGURES

CHAPTER 1: INTRODUCTION

Good inlet design is critical to the functioning of supersonic aircraft. The inlet cone must be positioned correctly for the oblique shock to impinge on the inlet wall (see Figure 1, below), such that internal instead of external compression occurs [1] and engine unstarts do not occur [2]. The inlet must be in the proper shape to offer the appropriate amount of subsonic air to the compressor. Lastly, the inlet should not be oversized for the amount of air it brings in, as this will increase the aircraft's cost, as well as its fuel consumption due to increased mass.

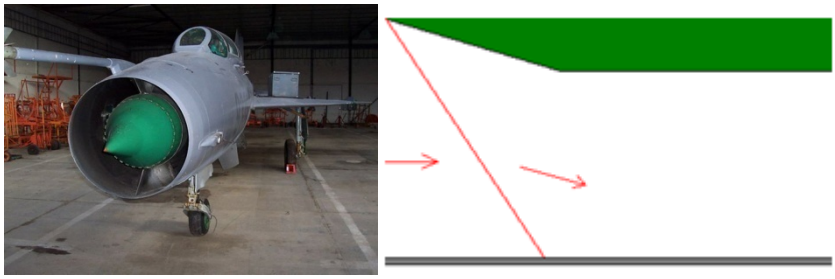

FIGURE 1. LEFT, A SUPERSONIC INLET. RIGHT, A SCHEMATIC SHOWING AN OBLIQUE SHOCK IMPINGING ON THE INLET WALL.

IMAGE SOURCE: TANKSFORSALE.CO.UK.

When an oblique shock generated by the inlet cone impinges on the inlet wall, a separation bubble forms. This is caused by the confluence of the oblique shock and a boundary layer that is formed on the inlet wall. Near the inlet wall, velocities will be subsonic, and zero at the wall itself due to the no-slip condition. Across an oblique shock, pressure increases, and the low momentum of the boundary layer air is insufficient to overcome this higher pressure. The flow separates as shown schematically in Figure 2 below.

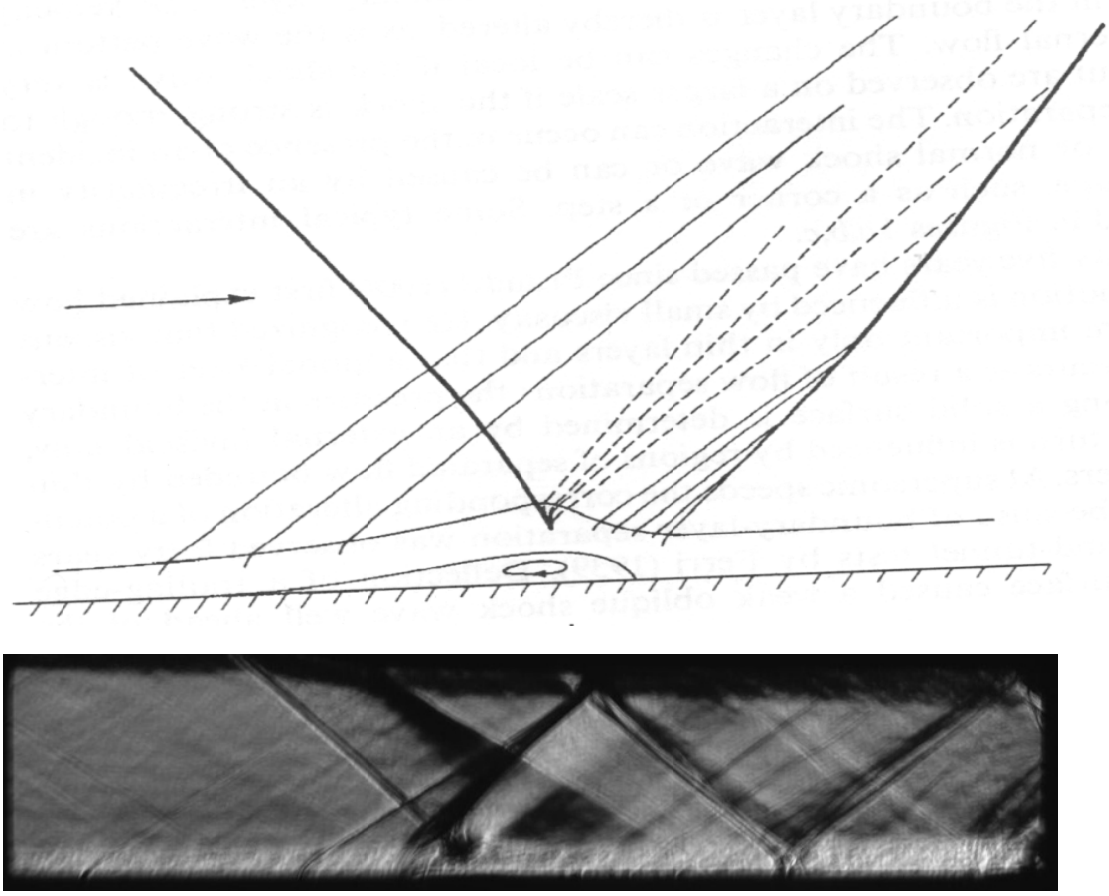

FIGURE 2. ABOVE, THE OBLIQUE SHOCKWAVE/BOUNDARY LAYER INTERACTION. NOTICE THE SEPARATED REGION, AND THE EXTRUDED BOUNDARY LAYER ABOVE IT. BECAUSE THIS EXTRUSION OCCURS AT THE OUTER RADIUS OF THE INLET, IT REPRESENTS A SIGNIFICANT WASTE OF INLET AREA. BELOW, A SCHLIEREN IMAGE OBTAINED EXPERIMENTALLY AS PART OF THIS RESEARCH.

TOP IMAGE SOURCE: [4].

As can be seen from the figure, the separation bubble formed by the oblique shockwave/boundary layer interaction causes the boundary layer to be extruded outward a significant distance. This represents a region air does not flow through but instead recirculates in. The corresponding inlet radius must be oversized by the height of the separation bubble, making the inlet larger and heavier.

There are two common ways to reduce the size of the oblique shockwave/boundary layer separation bubble. The first method is to bleed off some of the incoming boundary layer air. The low momentum air flows out through holes in the inlet wall and is lost. The air that replaces it comes from further away from the wall, and as such has higher momentum. The second method is to generate streamwise vortices. Once air is set rotating, the lower momentum air near the boundary layer rotates up towards the free stream, and the higher momentum free stream air moves downward into the boundary layer. The net result is that the air near the wall gains momentum, and separation is avoided or the separation bubble is reduced in size [3].

The use of plasma actuators to generate these vortices directly ahead of the oblique shockwave/boundary layer interaction was investigated. By using high voltage to ionize air and create arcs between positive and negative electrodes, plasma actuators are able to rapidly add amounts of thermal energy to the flow. The gas locally heats and expands, and because the flow is largely supersonic, the expanded gas generates a compression wave. It 'presses up' against the incoming flow, creating a virtual obstacle whose effect pulsates at the actuator firing frequency. This encourages the formation of streamwise vortices.

CHAPTER 2: LITERATURE REVIEW

The generation of vortices using micro-ramps was investigated by Anderson et al at NASA GRC [5]. Their tunnel test section consisted of a bottom flat plate, and a top 10° shock generator – essentially a radial cross-section of a supersonic inlet. To this, micro-ramps were added ahead of the separation region to encourage the formation of vortices. They found that it was possible to make the overall boundary layer equivalent to ordinary flat plate flow using these vortices (effectively eliminating the separation), though the momentum along the axis normal to the side of the tunnel was sinusoidal instead of even, owing to the vortical structures [5]. Figure 3 below shows their experimental setup.

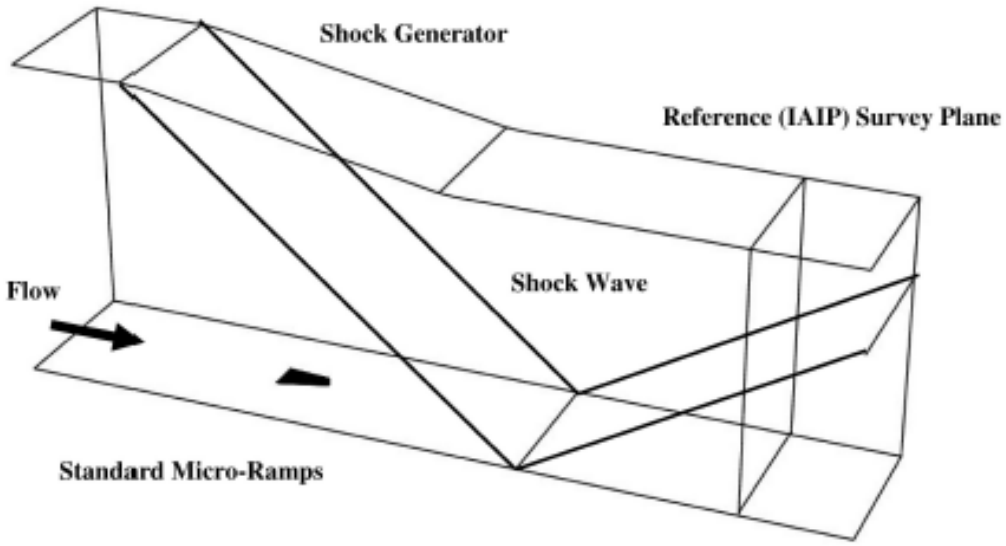

FIGURE 3. THE SETUP USED BY NASA GRC FOR THEIR MICRO-RAMP EXPERIMENTS.

IMAGE SOURCE: NASA GRC [5].

The effect of plasma actuators placed ahead of the shock generator was investigated by Leonov et al [6]. When activated, the actuators moved the shock forward, with angle

depending on power. While the study did not experiment with the oblique shockwave/boundary layer interaction, it did show that plasma actuators can act as 'virtual obstacles' and their effect is not just local, but instead can span the whole flow.

CHAPTER 3: EXPERIMENTAL SETUP

FACILITY

The wind tunnel used was a rectangular tunnel, 7.62 cm (3") wide and 3.81 cm (1.5") high. Various nozzle parts have been made for it, and the one selected for this project was a Mach 2 nozzle. Pressure to the tunnel is regulated by a control system. An analog pressure dial is installed on the control panel displaying total pressure, and static pressure is measurable via a tap installed on the side of the tunnel. From these two readings and assuming isentropic flow, the tunnel Mach number can be obtained:

$$M = \sqrt{\frac{2}{\gamma - 1}\left\{\left(\frac{p_0}{p}\right)^{\frac{\gamma-1}{\gamma}} - 1\right\}}$$

The Mach 2 nozzle used was tested and found to, in reality, produce a Mach 1.88 flow. This was achieved using a total operating pressure of 2.93 atm. Static pressure was measured to be 0.46 atm. While higher total pressures will also give Mach 1.88 flow, lower pressures deplete air tanks more slowly. The relationship between the total-static pressure ratio, mass flow rate and Mach number is shown in Figure 4 below.

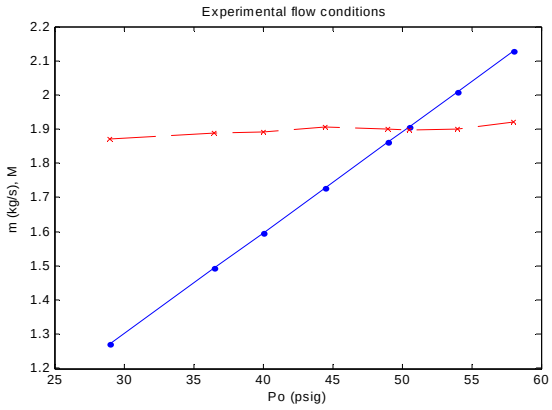

FIGURE 4. MASS FLOW RATE AND MACH NUMBER GIVEN VARIOUS TOTAL PRESSURES. THE NOZZLE LIMITS THE FLOW TO M=1.88.

PART DESIGN

TEST SECTION

To test plasma actuators' effect on the oblique shockwave/boundary layer interaction, first a wind tunnel test section had to be designed. So that results could be directly compared, like the NASA setup a 10° shock generator was chosen. The general arrangement is shown in Figure 5 below.

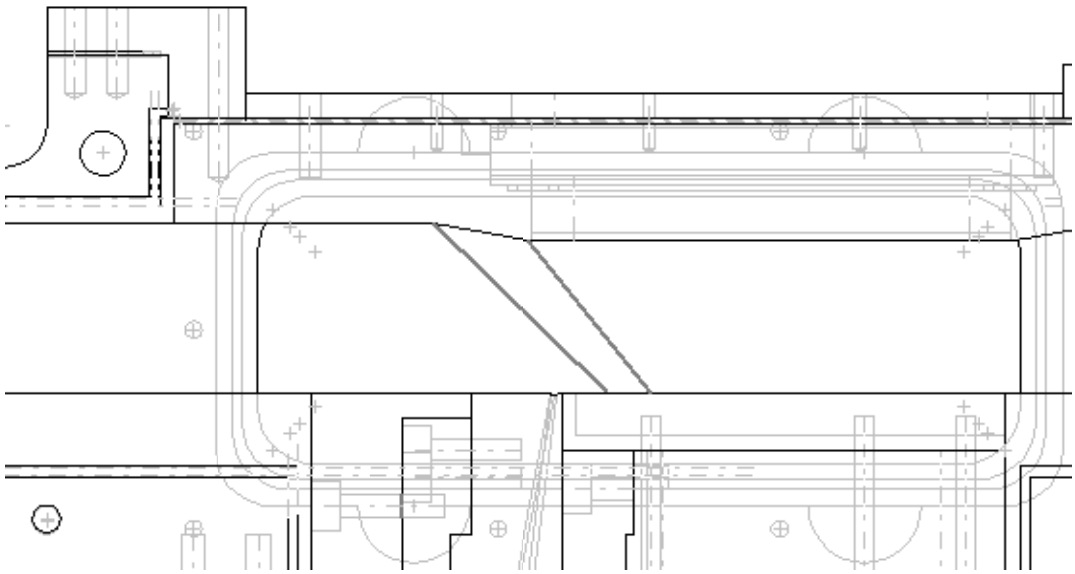

FIGURE 5. SIDE CROSS SECTION FOR THE DESIGNED WIND TUNNEL TEST SECTION. GRAY LINES IN THE MIDDLE INDICATE THE PATH OF THE FIRST OBLIQUE SHOCK, AS WELL AS THE START OF THE FOLLOWING EXPANSION FAN.

The height of the test section was determined by the requirement that the test section not choke the flow. Because total pressure goes down after the first oblique shock, it is possible for the flow to choke despite greater tunnel area than the nozzle. The design equation is:

$$A_{min.} = \frac{p_{01}}{p_{02}} A^*$$

Other dimensions were determined by practical considerations, such as ensuring that all windows could see the oblique shockwave/boundary layer interaction and the first reflection.

SHOCK GENERATOR

The shock generator piece was designed to be removable such that different shock generators could be tested without deconstructing the tunnel. To do this, the piece was designed as 7.52 cm (2.960") wide for the 7.62 cm (3") tunnel. This gave 0.05 cm (0.020") on each side, enough for a sliding fit. To seal the part, the O-ring groove was made wide enough to accommodate the uncompressed O-ring, but insufficiently high. When the part is being inserted into the tunnel, then, there is a 0.05 cm gap. When the top and bottom pieces of the test section are screwed in, they compress together. The area is insufficient to contain the O-ring, and so it presses out sideways, contacting the tunnel side wall and sealing it. Figure 6, below, shows the shock generator part, and Figure 7 demonstrates the operation of the O-ring in its grooves.

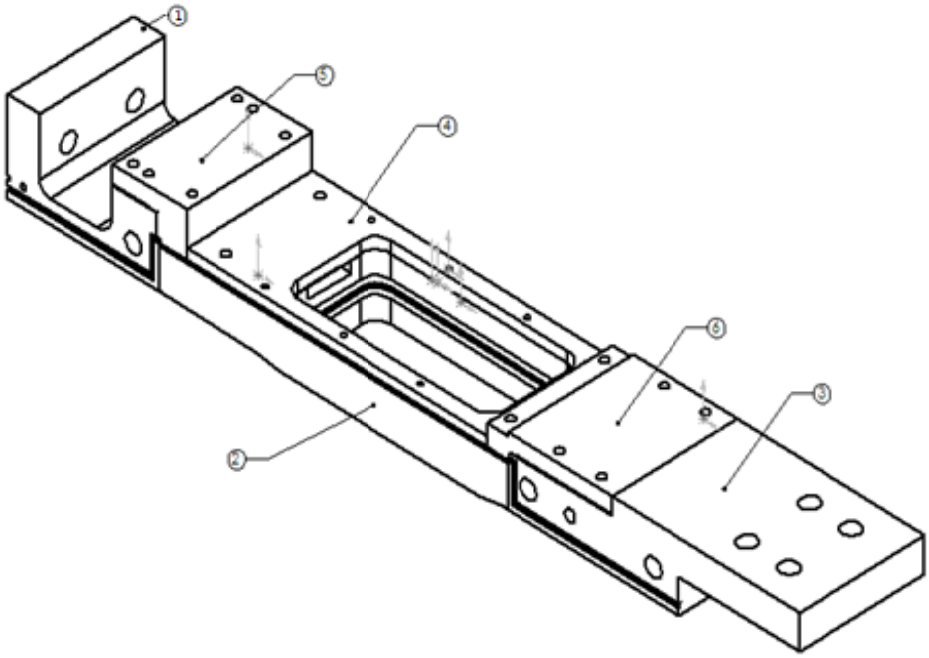

FIGURE 6. SHOCK GENERATOR PART. COMPONENTS: 1. TUNNEL-FRONT ATTACHMENT. 2. MAIN SHOCK GENERATOR. 3. TUNNEL-BACK ATTACHMENT. 4. TOP PART HOLDING WINDOW IN PLACE. 5. TUNNEL-FRONT-TO-MAIN. 6. TUNNEL-BACK-TO-MAIN.

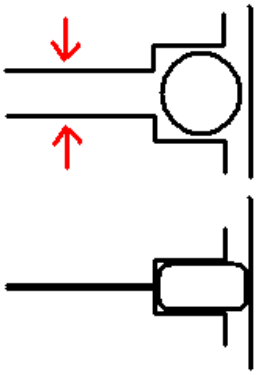

FIGURE 7. O-RING SEALING DESIGN.

FLOOR

The design of the floor was done by a graduate student, Edgar Caraballo. It was made to house an existing plasma actuator block, but such that the location of that block on the floor could be adjusted. To accomplish this, various blocks that attach on either side of the actuator block were created, such that the distance from the actuators to the oblique shock

impingement point could be configured as 0.25", 0.5", and 0.75". These blocks were designed to be held in place by screws. The design can be seen on the bottom side of Figure 5.

PLASMA ACTUATORS

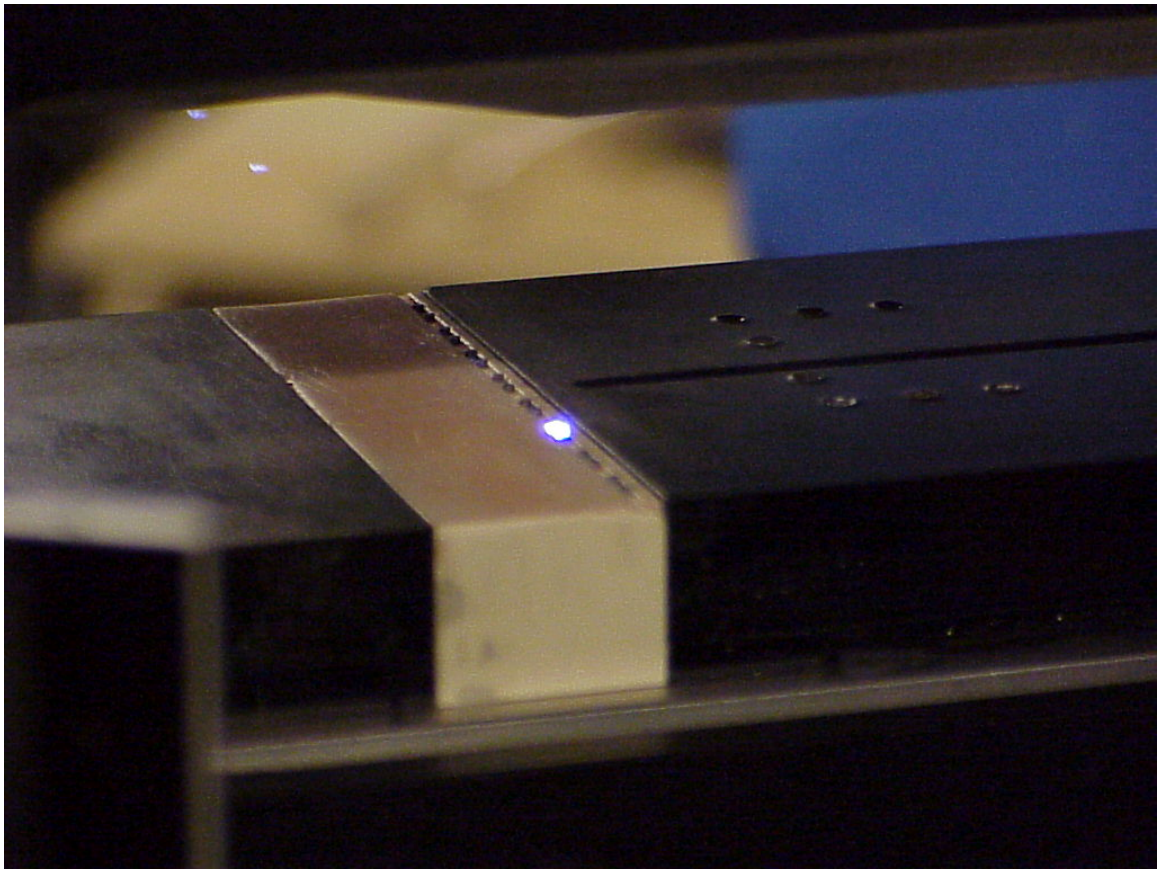

FIGURE 8. THE BORON NITRIDE PLASMA ACTUATOR BLOCK, SHOWN HERE WITH A SINGLE ACTUATOR FIRING.

The Boron Nitride plasma actuator block used holds eight plasma actuators, spaced 5 mm apart. Each actuator consisted of two tungsten electrodes – one positive and one negative, spaced 3 mm apart. These electrodes were powered by an actuator cart which provided high voltage, low current pulsed power. The actuator cart attached to a computer system

which allowed control over the phase of each individual actuator's firing, as well as the overall firing frequency.

COMPLETE TUNNEL

The tunnel, assembled with the test section installed, is shown below.

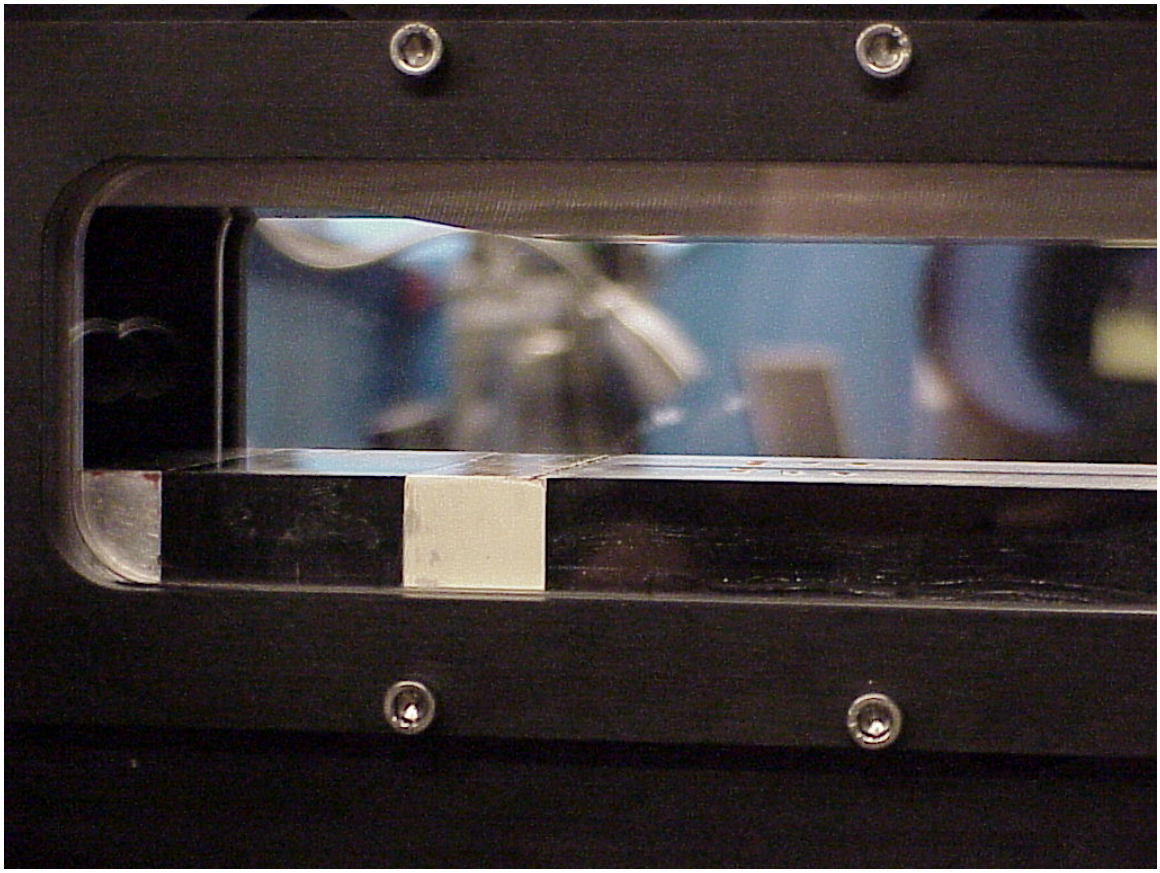

FIGURE 9. A CLOSE-UP OF THE WIND TUNNEL TEST SECTION, WITH SHOCK GENERATOR, FLOOR, AND PLASMA ACTUATORS INSTALLED.

FLOW VISUALIZATION

SCHLIEREN METHOD

Flow was visualized using schlieren photography. Schlieren photography is a technique that takes advantage of refractive index's dependence on density to visualize the flow density gradient. A series of mirrors are used to relay either pulsed or continuous collimated light from a light source, through the test section, to a convex mirror, and then to a knife-edge at a focus, and from there into a camera. To see why this configuration gives an image related to the gradient of the flow density, consider for simplicity a small angle approximation to Snell's Law:

$$\theta_2 = \frac{n_1}{n_2}\theta_1$$

Air's refractive index increases with density, so a beam of light entering a higher density region will have n1/n2 < 1, and will turn toward the higher density air. Likewise, entering a lower density region will mean n1/n2 > 1, and light will tend to bend away. Therefore, considering the vertical direction, if the air density is higher upward, light will bend slightly upward, and instead of being blocked it will reach the camera. Similarly if the air density is higher downward, the light will bend downward, and will be blocked instead of passing through the blade.

The end result is that, with schlieren photographs, high brightness indicates density increasing with height, and low brightness indicates density decreasing with height. This is why the leftmost oblique shockwave in Figure 2 is white on its bottom side, and black on its top side – it is denser than the rest of the flow. This is also why the top expansion fan is black – density, like pressure, drops during supersonic acceleration. Were the expansion fan on the bottom side, it would be white.

The schlieren system can capture data in two modes, continuous and instantaneous. In continuous mode, light is always provided, causing the camera to get an average picture of the flow. It is easy to see the general shape of the flow in this mode, but the averaging process hides details. In instantaneous mode, argon is supplied at low pressure to the light source, which uses it to emit bright pulses of light. Despite the short duration of the pulse, the incoming light is so intense that the camera's sensors receive as much energy as they would in a normal frame, allowing an image to be captured averaging over a far shorter time slice than the camera can ordinarily capture. These images show high frequency details that are impossible to notice otherwise. The light source is shown below.

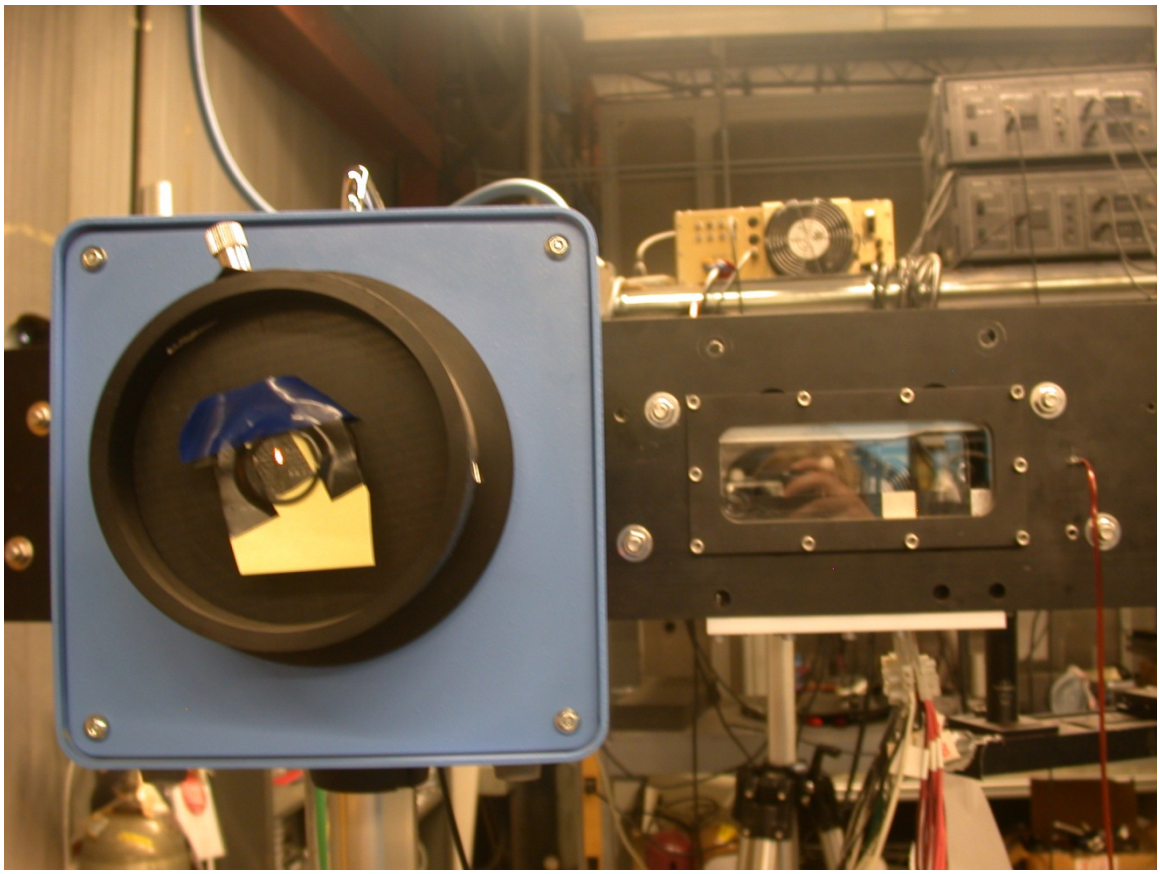

FIGURE 10. LIGHT SOURCE FOR SCHLIEREN IMAGING.

CHAPTER 4: EXPERIMENTAL METHODOLOGY

MEASURING PRESSURE

To verify that the shock generator was working properly, a pressure tap was installed in the side of the wind tunnel, upstream of the test section – Port 1. Additionally, a side window was installed with four pressure ports, the first before the shock location, the second was in the shock region, and the third and fourth were after the shock. These were Ports 2-5. Because all of these pressure taps were on the side of the tunnel, they measured static pressure.

Total pressures from 29 to 58 psig were tested to find the pressure required such that the static pressure after the shock was 0 psig – atmospheric pressure. By doing this, the effect of any possible leaks was minimized.

SCHLIEREN IMAGING

Schlieren images were captured in continuous mode for diagnostic purposes, such as checking the cleanliness of the flow. They were not used with the plasma actuators activated.

In pulsed mode, sets of ten images were taken with plasma actuators off, and firing at 1, 3, 5, 7, 9 or 11, 15, 20, 25, 30, and 40 kHz, as well as phase-locked 5 kHz. Images were captured once per second. Three actuator-to-shock impingement point distances were tested – 0.25”, 0.5”, and 0.75”.

To make it easier to detect subtle differences between the schlieren images, the sets of ten were first averaged. The average intensity of the image (excepting extreme dark and light) was taken, and the image was normalized such that the average intensity was always 50%

brightness. The difference between each individual picture and a baseline picture was then calculated. Where the pictures matched in intensity, the resulting difference picture was made 50% gray. Where the picture was brighter than the baseline, the resulting picture was brighter, and the same principle applied where the picture was darker. In this manner it was possible to see if there were significant changes from the baseline case.

CHAPTER 5: RESULTS

STATIC PRESSURE MEASUREMENTS

Static pressures for Ports 1-5 as measured for various total pressures are shown below.

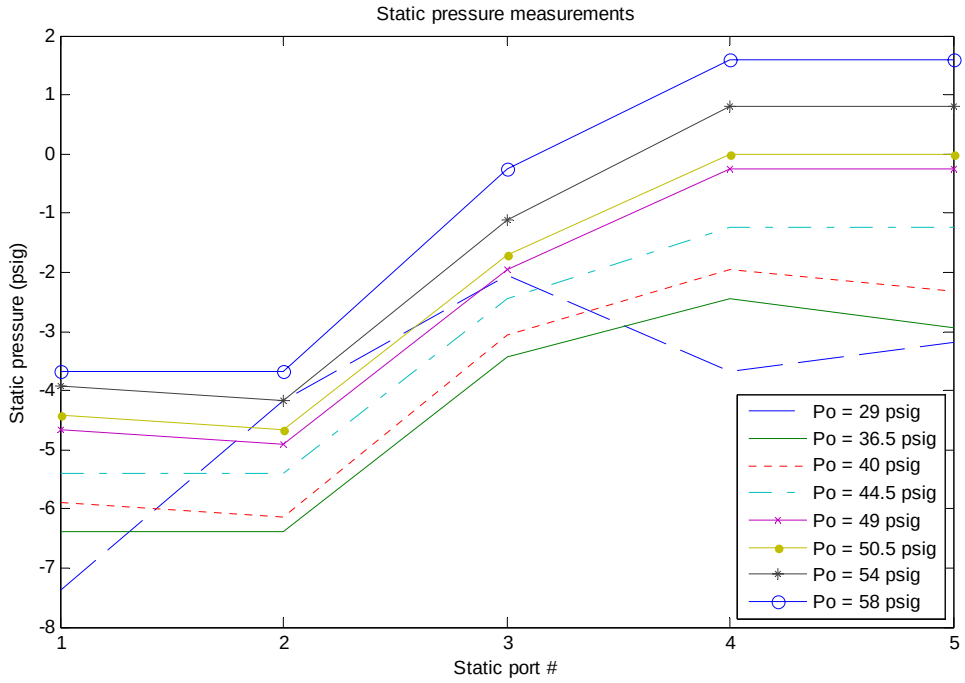

FIGURE 11. STATIC PRESSURES WITH SHOCK GENERATOR IN PLACE.

Atmospheric pressure after the shock is achieved at 49 psig. As a result, experiments were carried out at this pressure.

FLOW IMAGES

Results for baseline, 1 kHz, 5 kHz, and 9 or 11 kHz are shown below for 0.25”, 0.5”, and 0.75” shock distances. Additional images are in the Appendix.

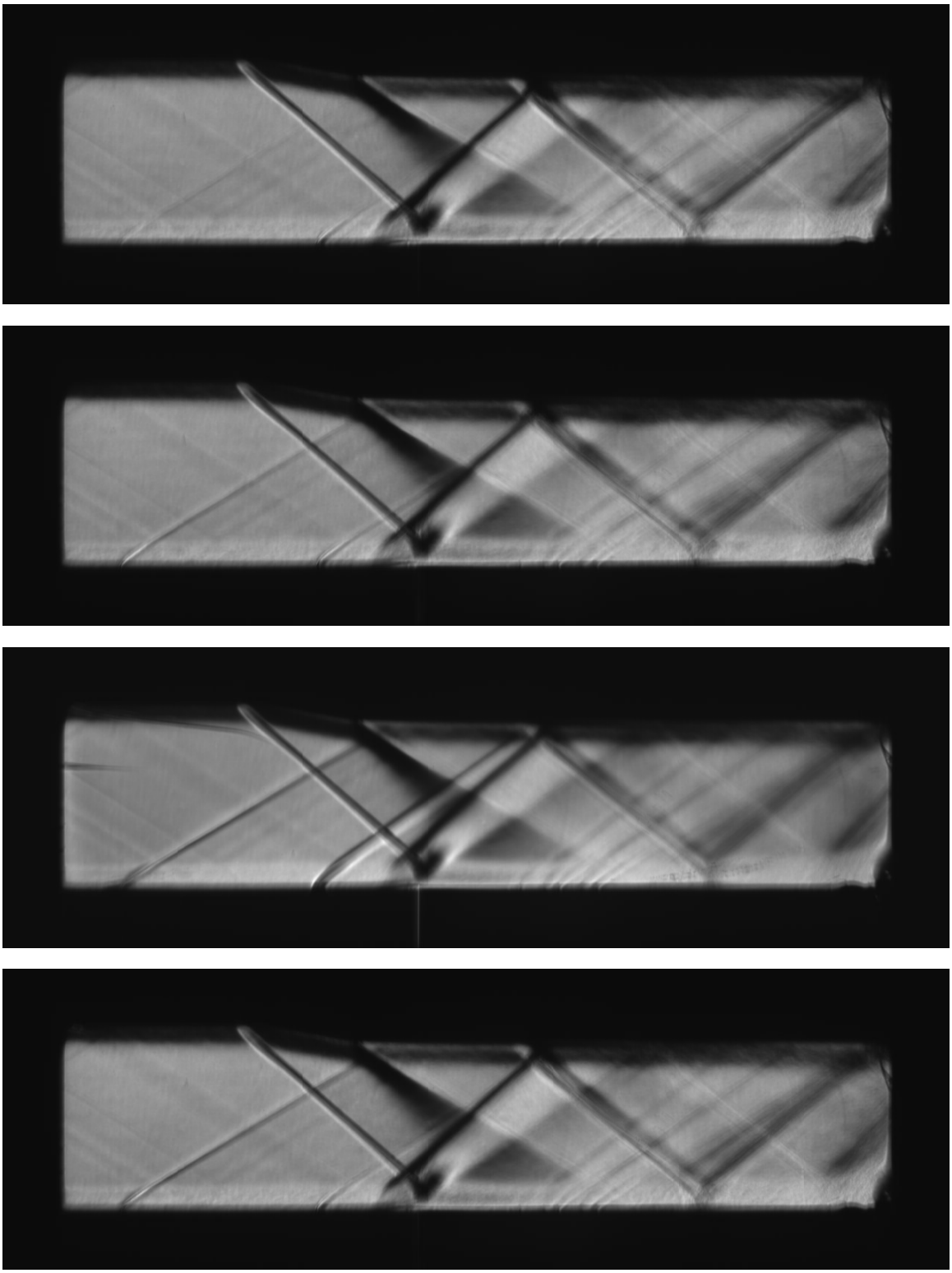

FIGURE 12. BASELINE, 1 KHZ, 5 KHZ, AND 11 KHZ FOR 0.25" SHOCK DISTANCE. THE UNUSUAL EARLY SHOCK AT 5 KHZ IS LIKELY DUE TO THERMAL CONTRACTION OF THE ALUMINUM FLOOR INSTEAD OF THE ACTUATORS.

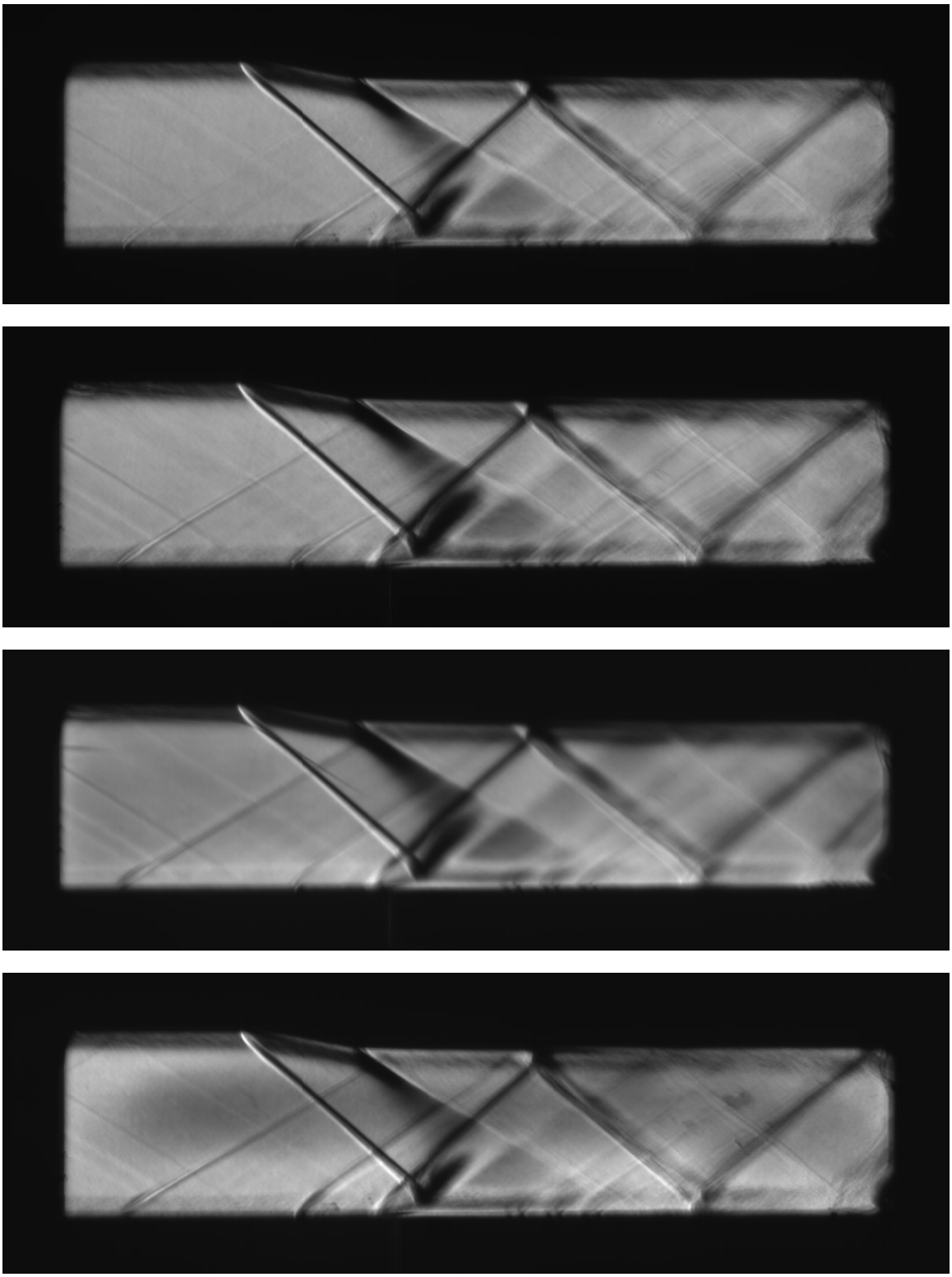

FIGURE 13. BASELINE, 1 KHZ, 5 KHZ, AND 9 KHZ FOR 0.5" SHOCK DISTANCE.

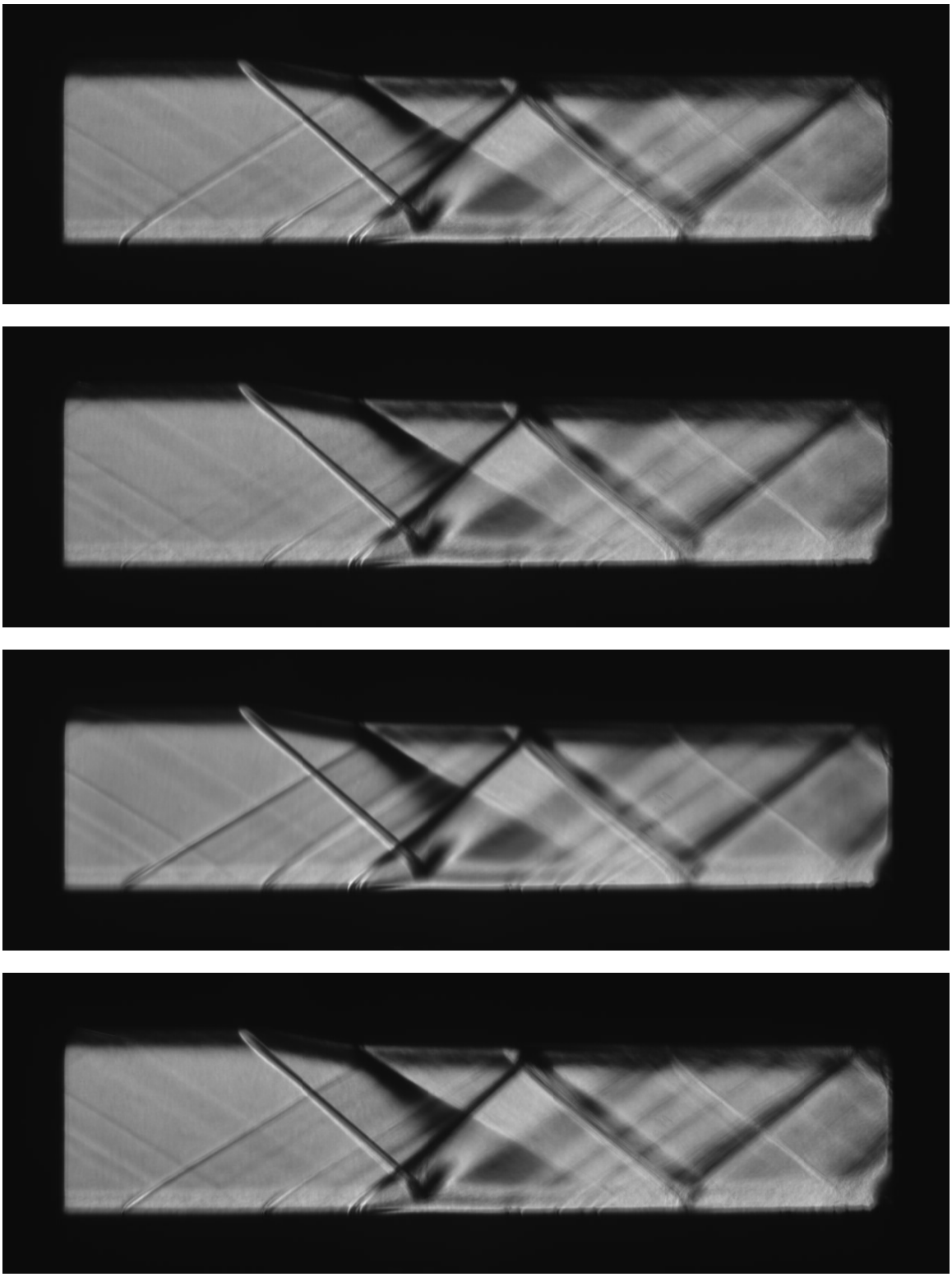

FIGURE 14. BASELINE, 1 KHZ, 5 KHZ, AND 11 KHZ FOR 0.75" SHOCK DISTANCE.

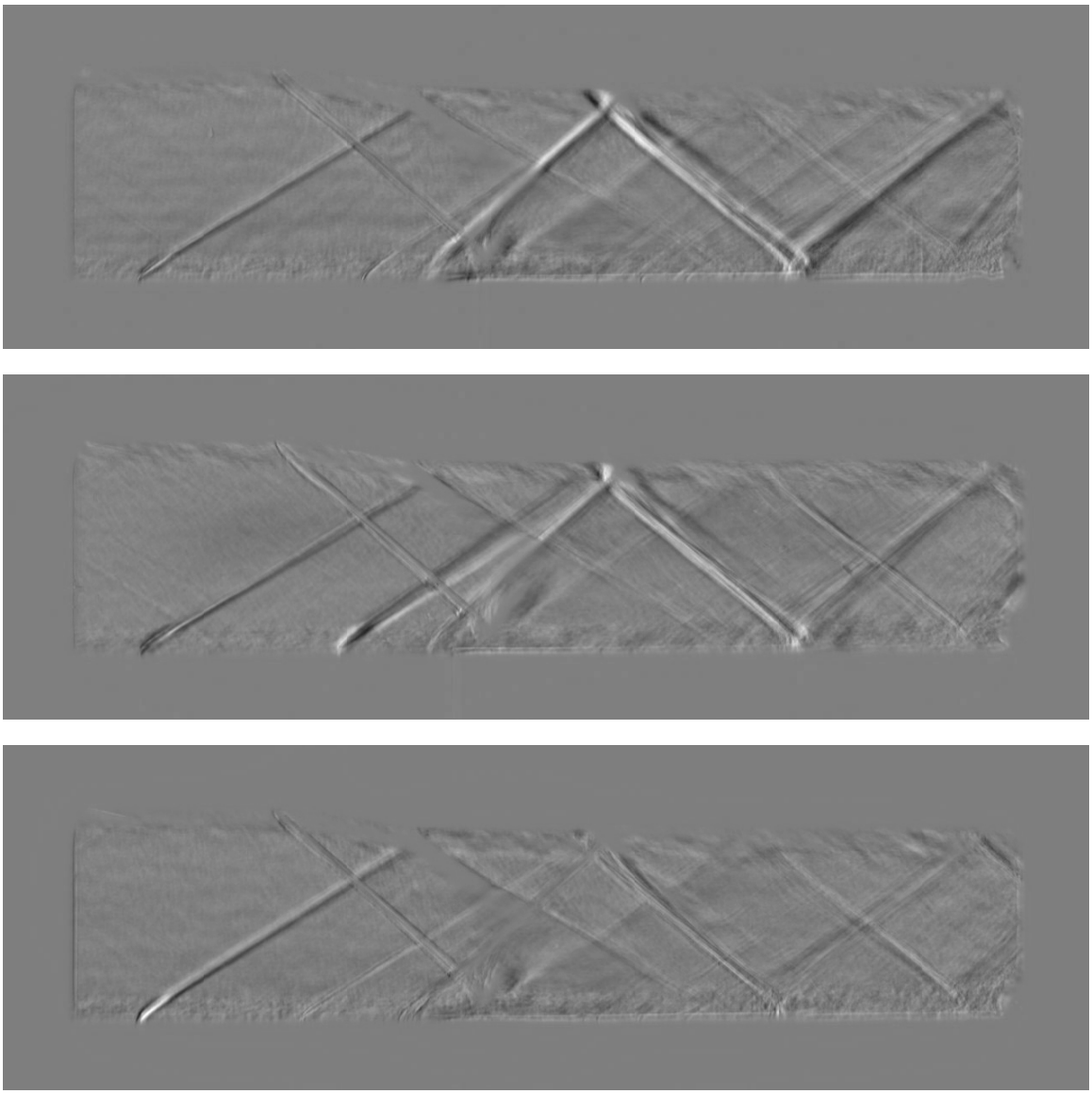

FIGURE 15. 7 KHZ DIFFERENCE IMAGES FROM BASELINE FOR 0.25", 0.5", AND 0.75" SHOCK DISTANCES.

CHAPTER 6: DISCUSSION

The shock generator works as expected, and the separation bubble is also visible. However, it is very hard to see differences between the tested actuator frequencies, or even between the tested actuator-to-shock impingement distances. From the differenced flow images, one can see that a weak initial shock appears at 7 kHz that does not exist in the baseline case. This is likely due to thermal contraction of the aluminum floor over the duration of the tunnel run. Near the interaction region, there appear to be slight differences, but they are not the same for each shock distance so it is hard to make any general conclusion.

While schlieren images are good for seeing the overall flow, the three dimensional nature of vortices in an oblique shockwave/boundary layer interaction [3] may mean that the details necessary to see an effect are being averaged out in the axis normal to the side windows. Along this axis, NASA's work with micro-ramps found a wavy momentum distribution. Assuming that the effect of plasma actuators is similar, determining whether the momentum distribution contains these upwash and downwash regions would be a good way to know if the actuators are adding significant vorticity.

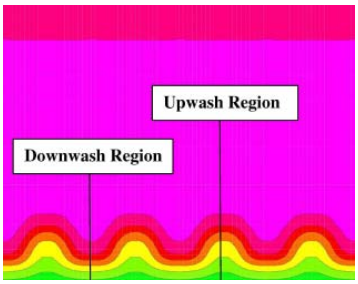

FIGURE 16. WAVY MOMENTUM DISTRIBUTION.

IMAGE SOURCE: NASA GRC [5]

At the present time, one can conclude that either the flow is three dimensional and the actuators' effect is being averaged out, or there is very little effect.

CHAPTER 7: CONCLUSION

The wind tunnel test section worked as designed, generating oblique shocks which impinged at the design locations. No significant leakage of air occurred, except due to thermal contraction of the aluminum floor after prolonged use of the tunnel.

Using only schlieren images, plasma actuators do not appear to have a significant effect. However, this may be because the visualizations are two-dimensional averages of a three-dimensional phenomenon.

To get quantitative measurements of the differences between the baseline and actuated cases, the use of Particle Image Velocimetry would be beneficial. Pressure measurements on the floor after the separation bubble should also be taken to determine if the pressure distribution is even or if it suggests a wavy momentum distribution. By doing both of these things, it will be possible to determine what effects the plasma actuators are having.

APPENDIX

PHASE-LOCKED 5 KHZ FLOW IMAGES

0.25” ACTUATOR DISTANCE

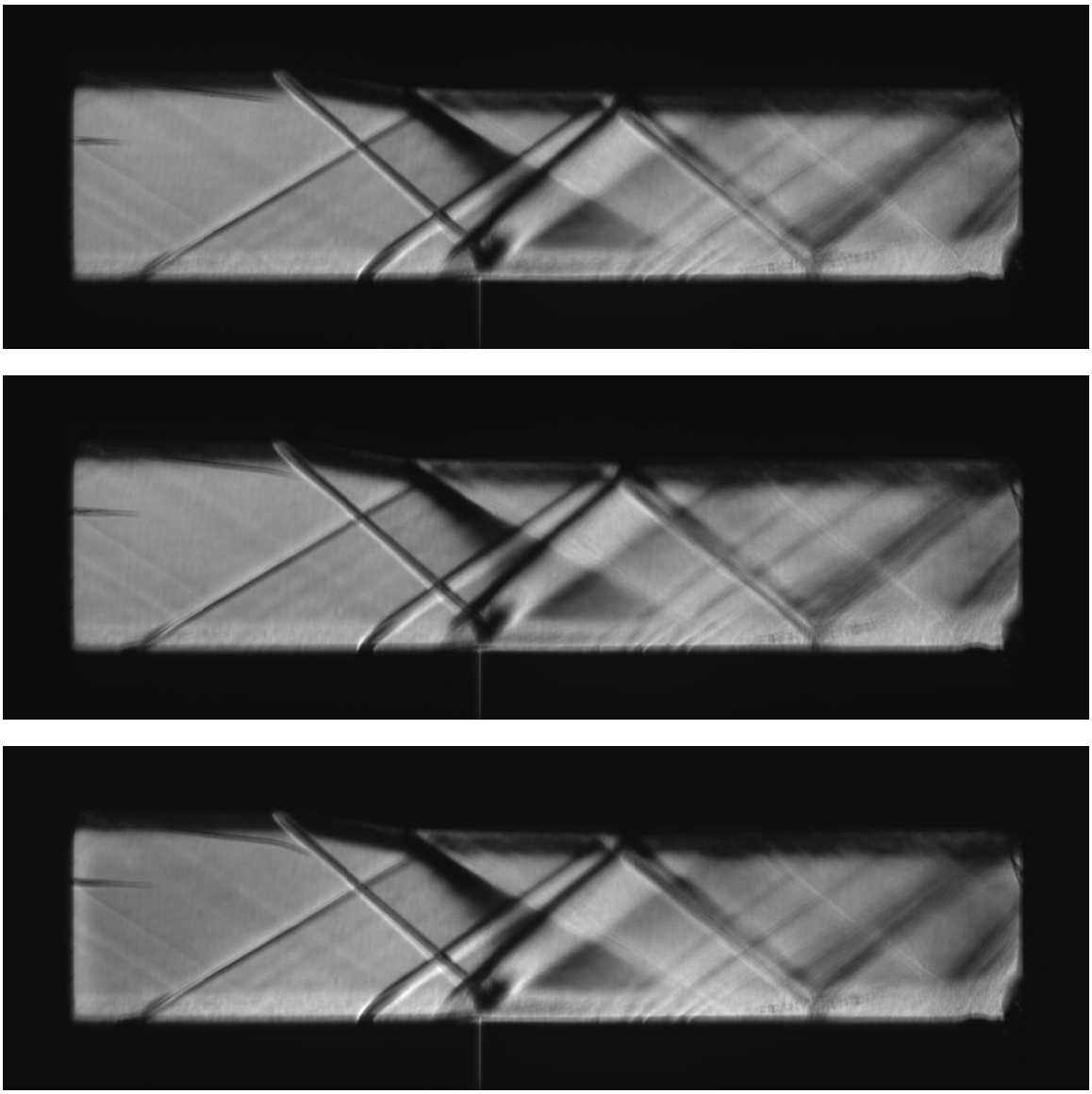

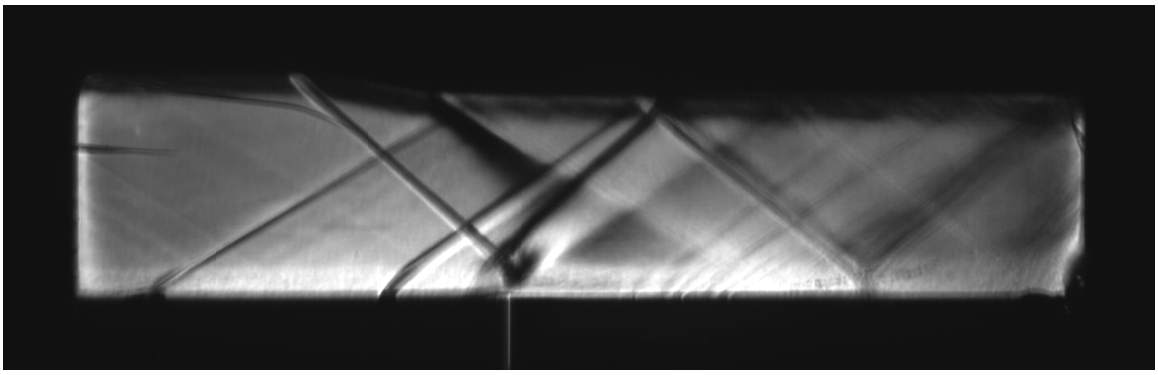

FIGURE 17. 0°, 90°, 180°, AND 270° PHASE AT 0.25”.

0.5” ACTUATOR DISTANCE

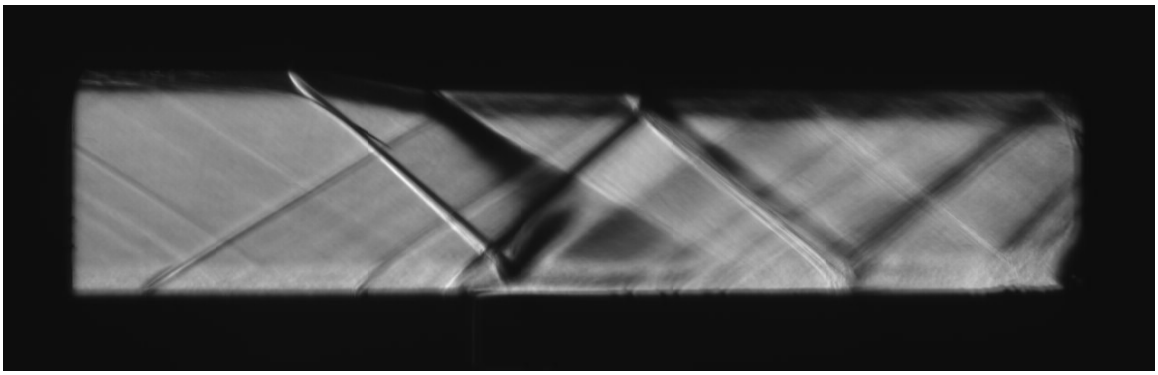

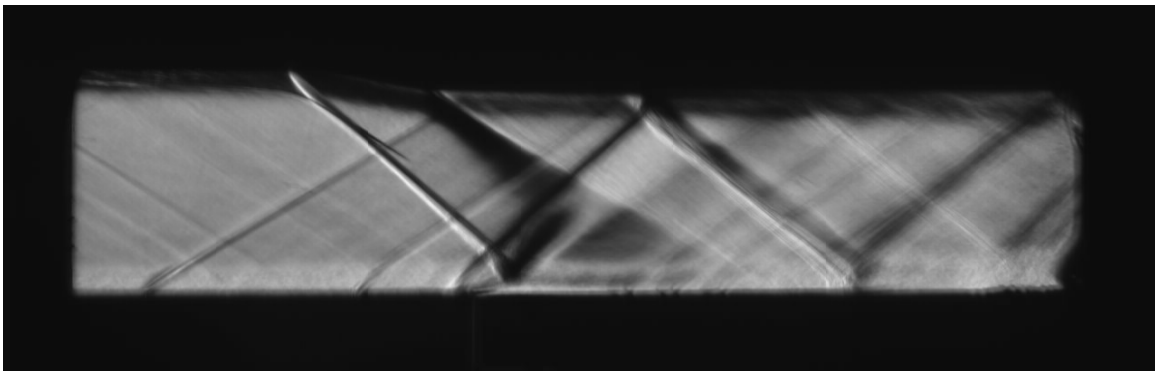

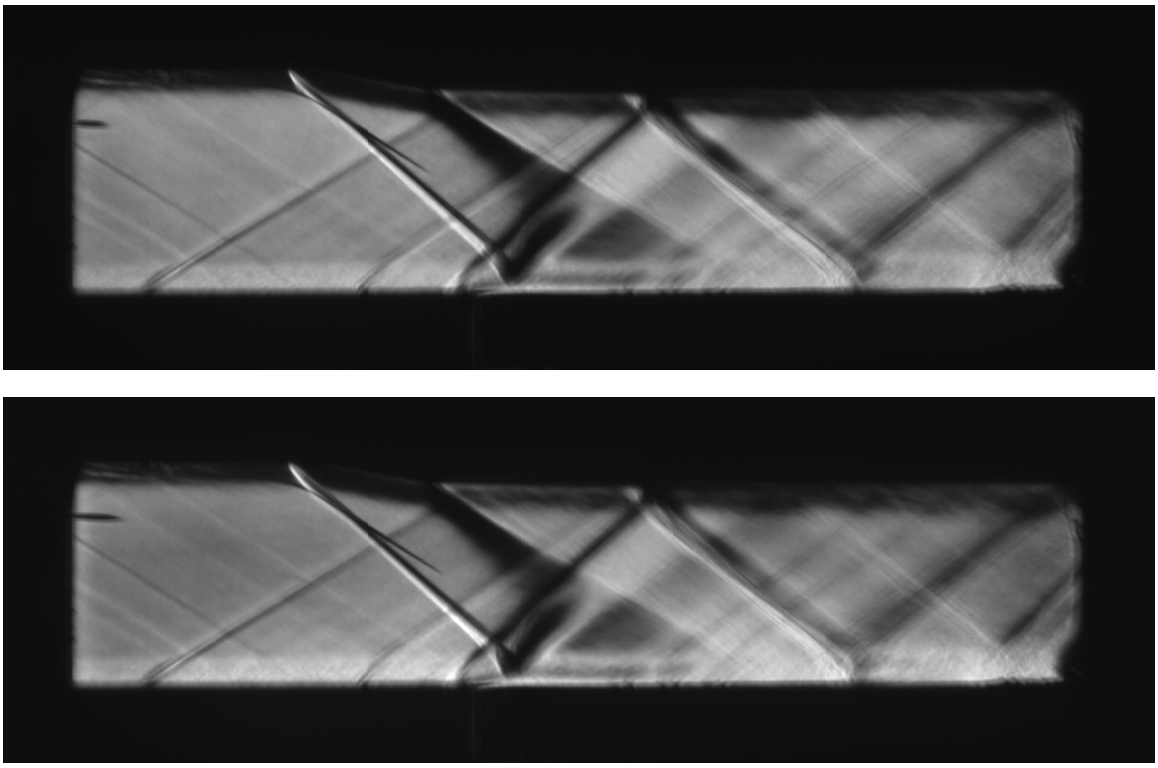

FIGURE 18. 0°, 90°, 180°, AND 270° PHASE AT 0.5”.

0.75” ACTUATOR DISTANCE

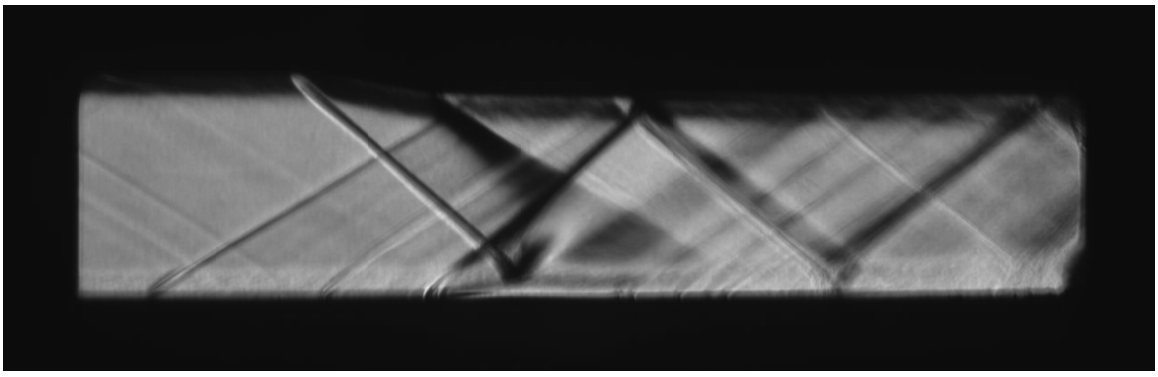

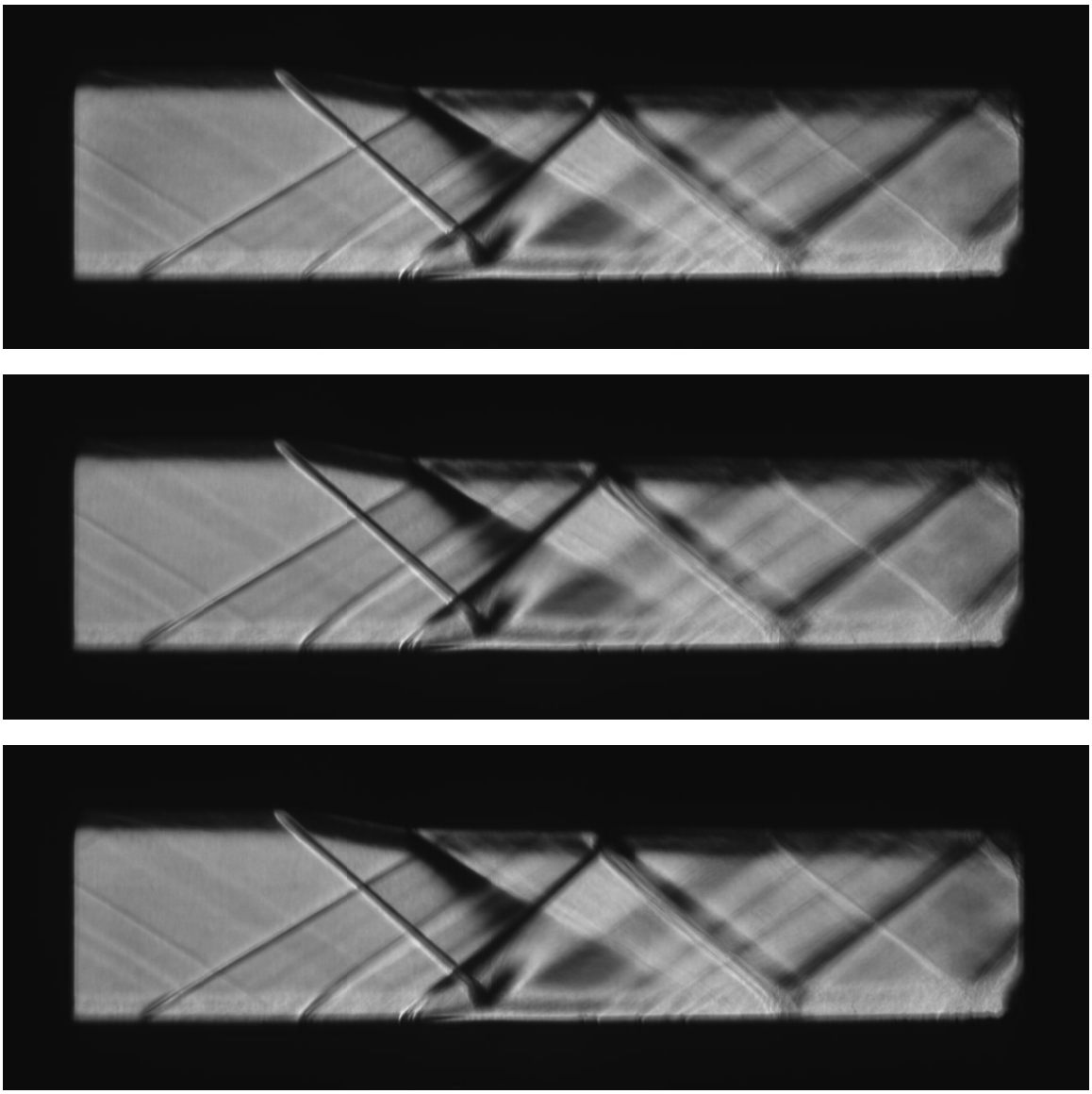

FIGURE 19. 0°, 90°, 180°, AND 270° PHASE AT 0.75”.

REFERENCES

[1] "Inlet cone." Wikipedia. http://en.wikipedia.org/w/index.php?title=Special:Cite&page=Inlet_cone&id=200594489

[2] Discussion with Dr. Michael Dunn, The Ohio State University.

[3] Holger Babinsky. "Micro-ramp control of inlet flows." *NASA Workshop on Shock Wave/Boundary Layer Interaction*. April 2002.

[4] T. C. Adamson, Jr. and A. F. Messiter. "Analysis of Two-Dimensional Interactions between Shock Waves and Boundary Layers." *Ann. Rev. Fluid Mech. 1980.*

[5] Bernhard H. Anderson, Jon Tinapple and Lewis Surber. "Optimal Control of Shock Wave Turbulent Boundary Layer Interactions Using Micro-Array Actuation." 3rd *AIAA Flow Control Conference*. June 2006. NASA/TM—2006-214373. AIAA—2006-3197.

[6] Sergey B. Leonov, Dmitry A. Yarantsev, and Victor R. Soloviev. "Experiments on Control of Supersonic Flow Structure in Model Inlet by Electrical Discharge." 37th *AIAA Flow Control Conference.* June 2007. AIAA—2007-3890.